


## Interrupted Motility Induced Phase Separation in Aligning Active Colloids

Marjolein N. van der Linden,<sup>1,2</sup> Lachlan C. Alexander,<sup>2</sup> Dirk G. A. L. Aarts,<sup>2</sup> and Olivier Dauchot<sup>1</sup>

<sup>1</sup>*Gulliver UMR CNRS 7083, ESPCI Paris, PSL Research University, 10 rue Vauquelin, 75005 Paris, France*

<sup>2</sup>*Physical and Theoretical Chemistry Laboratory, Department of Chemistry-University of Oxford, South Parks Road, Oxford OX1 3QZ, United Kingdom*

 (Received 21 February 2019; revised manuscript received 19 May 2019; published 28 August 2019)

Switching on high activity in a relatively dense system of active Janus colloids, we observe fast clustering, followed by cluster aggregation towards full phase separation. The phase separation process is however interrupted when large enough clusters start breaking apart. Following the cluster size distribution as a function of time, we identify three successive dynamical regimes. Tracking both the particle positions and orientations, we characterize the structural ordering and alignment in the growing clusters and thereby unveil the mechanisms at play in these regimes. In particular, we identify how alignment between the neighboring particles is responsible for the interruption of the full phase separation. Our large scale quantification of the phase separation kinetics in active colloids points towards the new physics observed when both alignment and short-range repulsions are present.

DOI: [10.1103/PhysRevLett.123.098001](https://doi.org/10.1103/PhysRevLett.123.098001)

Self-propelled particles show a strong tendency to phase separate or form clusters with various structural and dynamical properties [1–30]. Two limiting scenarios have been identified. When alignment dominates the interactions, a transition to polar or nematic order takes place following a phase separation between a disordered gas and an orientationally ordered liquid. At coexistence, polar bands or nematic lanes dominate the dynamics. This physics is captured in Vicsek-like models [31–34]. When excluded volume interactions dominate and crowding effects slow down the propulsion speed, a motility-induced phase separation (MIPS) takes place: coarsening leads to the formation of one large droplet surrounded by a disordered gas phase [9,14,16]. Both scenarios are well understood at the level of large-scale hydrodynamic equations [35–37].

In experimental situations, clustering results from the interplay of several factors such as self-propulsion, excluded volume, alignment and noise, in addition to usual attractive, repulsive and hydrodynamic interactions. Disentangling these effects is a truly challenging task [38] that has motivated a large number of numerical studies [17,22,23,25,26,28,29]. Of particular interest, is the case where alignment and excluded volume are simultaneously present. These are the minimal ingredients at play in the population dynamics of elongated microorganisms [4,24,39–42]. On one hand, it was argued that alignment reduces the rotational diffusion and therefore favors MIPS [28,29]. On the other hand, recent simulations of self-propelled rods suggest that steric alignment reduces MIPS to a minor part of the phase diagram [30], in agreement with earlier simulations [5,21].

In this Letter, we take advantage of a 2D experimental system of induced-charge electrophoretic self-propelled

Janus colloids [43,44] to study the clustering and coarsening processes (Fig. 1). We specifically focus on the aggregation kinetics and demonstrate that (i) initially, single particles aggregate into clusters, the size of which rapidly increases, first exponentially with alignment playing no role, then following a power law with an exponent prescribed by the Cahn-Hilliard equation, (ii) later, a second regime of aggregation-fragmentation takes place, during which cluster dynamics, composed of rigid body translation and rotation, is dominated by the orientational ordering of the colloids inside the clusters, and (iii) finally, the phase separation is eventually interrupted when fragmentation events dominate. It is the intricate

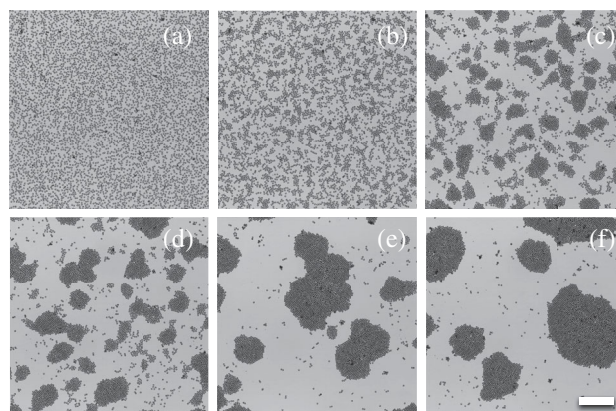


FIG. 1. Aggregation kinetics in a system of induced-charge electrophoretic self-propelled Janus colloids: From (a) to (f) : Successive time steps ( $t = 0.02, 0.4, 2, 5, 20, 68$  s) following the onset of activity. Scale bar is  $100 \mu\text{m}$ . See also Movie-1 in the Supplemental Material [45].

interdependence of the structural and polar ordering growth that controls the kinetics. In particular in the last regime, the largest clusters break up along grain boundaries, which were formed during their aggregation. These regions populated with defects cannot resist the active stresses resulting from the partial alignment within the grains.

The experimental system, following Ref. [44], is composed of tens of thousands of Janus colloids (silica particles with a diameter  $d$  of  $4.28 \mu\text{m}$  half coated in  $35 \text{ nm}$  of titanium followed by  $15 \text{ nm}$  of silica) in an aqueous solution of  $0.1 \text{ mM}$  NaCl, sandwiched between two ITO cover slips (Diamond Coatings) that were coated with  $25 \text{ nm}$  of silica, separated by  $\sim 95 \mu\text{m}$  thick spacers. The particles form a monolayer, with a surface fraction  $\phi \simeq 0.25$ , on the bottom electrode. When a square wave with a frequency of  $10 \text{ kHz}$  and an amplitude of  $10 \text{ V}$  is applied, the particles self-propel with their silica side facing forward, as prescribed by induced-charge electrophoresis (ICEP) [46]. We record the dynamics at  $50 \text{ fps}$  using an Olympus Plan N  $20 \times /0.40$  objective and  $2048 \times 2048$  pixels camera. This allows us to capture the large scale dynamics, while simultaneously tracking the particles positions  $\mathbf{r}_k(t)$  and orientations  $\mathbf{n}_k(t)$ . The nominal velocity of an individual particle is  $v_0 \simeq 20d/s$ . For such large particles, the rotational diffusion constant  $D_R \simeq 10^{-2} \text{ s}^{-1}$  so that the persistent length of the trajectories  $l_p = v_0 D_R^{-1} \simeq 2000d$ . At the working frequency, the dielectric dipole-dipole interactions are weak [44]. A visual inspection of pairwise interactions (see Movie 5 to 8 in the Supplemental Material [45]) however reveals a short-range repulsion (particles never strictly collide), together with some head-to-tail attraction. As a result particles incoming sideways align their directions almost perfectly, while particles colliding head-on do not align. The total number of particles  $M$  inside the field of view remains approximately constant ( $M \simeq 5500$ ).

In a typical run [45], clustering starts right at the onset of self-propulsion. Clusters are defined using a nearest neighbor criteria, with a cutoff distance  $1.2d$ . Figures 2(a), 2(b) display the average cluster size, defined as  $\langle s \rangle = \{1/[N(t)]\} \sum_i s_i$ , with  $N(t)$  the number of clusters at time  $t$  and  $s_i$  the number of colloids inside cluster  $i$ , and the fraction of particles inside clusters of increasing size. One readily distinguishes three regimes. At short time  $t < 2 \text{ s}$ , isolated particles aggregate in small clusters of average size  $\langle s \rangle < 10$  and maximal size  $s_{\text{max}} \simeq 250$  (regime I). The transition to the second regime is marked by the abrupt slowing down of the coarsening, when most of the individual particles have aggregated.  $\langle s(t) \rangle$  remains flat for another  $2 \text{ s}$  before coarsening resumes via a complex fragmentation-aggregation dynamics (regime II). Finally, the phase separation is interrupted at long times ( $t = 20 \text{ s}$ ), leading to a regime dominated by strong fluctuations of the average cluster size around  $\langle s \rangle = 30$ , with  $s_{\text{max}} \simeq 2000$  (regime III).

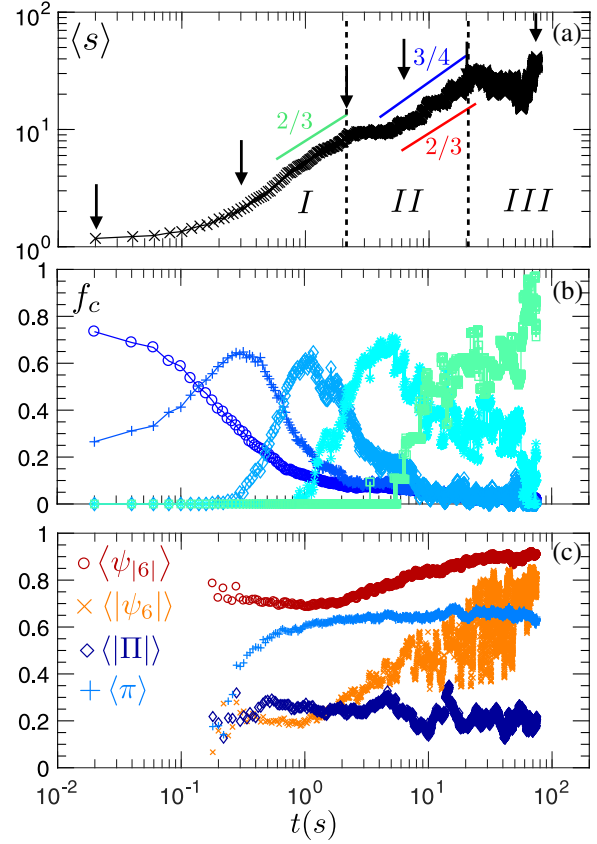


FIG. 2. Cluster size and order parameters: (a) Average cluster size versus time; the arrows point at the times of the snapshots shown on Fig. 1; the vertical dashed lines separate the three dynamical regimes described in this Letter. (b) Fraction of particles inside clusters of size  $(\circ) s = 1, (+) s \in [2, 19], (\diamond) s \in [20, 99], (*) s \in [100, 499], (\square) s \in [500, 4999]$ . (c) Weighted average of the hexagonal  $\psi_{|6|}$ , hexatic  $|\psi_6|$ , aligning  $\pi$ , and polar  $|\Pi|$  order parameters (see text for definitions).

When the clusters form, they rapidly develop hexagonal order, and polar alignment of the particles. Figure 2(c) reveals how structural and polar order develops. For each cluster of size  $s$ , the structural order is characterized using the hexagonal, respectively, hexatic, order parameter  $\psi_{|6|} = (1/s) \sum_{k=1}^s |\psi_{6,k}|$ , respectively,  $|\psi_6| = |(1/s) \sum_{k=1}^s \psi_{6,k}|$ , where  $\psi_{6,k} = (1/N_k) \sum_{j=1}^{N_k} \exp(6i\theta_{jk})$ , with  $\theta_{jk}$  the orientation of the link connecting two neighboring particles, and the sum runs over the  $N_k$  nearest neighbors of particle  $k$ , using a cutoff distance of  $1.2d$ . The alignment is defined as  $\pi = (1/s) \sum_{k=1}^s \pi_k$ , with  $\pi_k = (1/N_k) \sum_{j=1}^{N_k} \mathbf{n}_j \cdot \mathbf{n}_k$ . The polarity of a cluster of size  $s$  is given by  $|\Pi| = |(1/s) \sum_{k=1}^s \mathbf{n}_k|$ . Figure 2(c) is obtained by averaging over clusters with  $s \geq 7$  present at time  $t$ , weighting the average with the cluster size. One readily sees that the different orders develop at different pace. In the following we shall describe the three growth regimes, focusing on the interplay between structure, polar ordering, and growth. In the first regime, we base our analysis on the statistics of the cluster

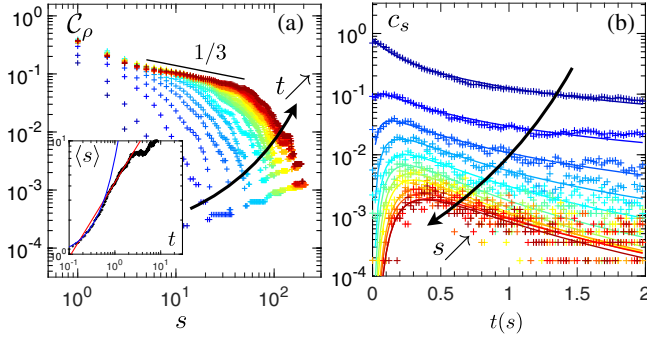


FIG. 3. Regime I, statistics of sizes: (a) Cumulative distribution of the cluster size,  $\mathcal{C}_\rho(s, t)$ , for increasing times  $t \in [0, 2]$  s every 0.2 s (from blue to red); inset :  $\langle s(t) \rangle$ ; the continuous blue line is an exponential fit  $e^{t/t_1}$ , with  $t_1 = 25$  s; the continuous red line is a power law fit  $t^{-\gamma}$ , with  $\gamma = 2/3$ . (b) Cluster size histogram  $c_s(t)$  as a function of time, for  $s \in [1, 12]$ ; the continuous lines are fits of the form  $h(t) \propto \{[(t/t_2)^{p(s)}]/[(1 + t/t_2)^{q(s)}]\}$ , with  $t_2 = 10$  s,  $p(s) = 0.6(s - 1)$ , and  $q(s) = s - 1$  (see text for details).

size. At longer times we concentrate on the structure and orientational organization of the clusters to identify the reasons for the interruption of the coarsening process.

**Regime I: Clustering.**—The initial aggregation follows a standard route, akin to equilibrium aggregation: the cluster size distribution  $\rho(s, t)$  is exponential at very short times and progressively develops a power law regime. This is best illustrated by the cumulative distribution  $\mathcal{C}_\rho(s, t) = \int_s^\infty du \rho(u, t)$  plotted at successive times on Fig. 3(a), from which we infer that  $\rho(s, t) \propto s^{-\alpha} \exp[-s/s^*(t)]$ , with  $\alpha \lesssim 4/3$ , smaller than the typical values  $\alpha \in [1.7, 2]$  [6, 19, 27, 47], indicating a truly broad distribution of sizes. The crossover size  $s^*$  sets the average cluster size  $\langle s \rangle$ , the evolution of which is displayed in the inset. The initial exponential growth, expected for an aggregation instability, coincides with the formation of branched clusters [see Fig. 1(b)]. This initial regime is followed by a power law growth of the cluster size  $\langle s \rangle \sim t^{\gamma_1}$ , with  $\gamma_1 \simeq 2/3$ , during which the clusters rapidly become rather compact. The characteristic length  $\mathcal{L}$  associated with the clusters growth thus follows  $\mathcal{L} \sim t^{1/3}$ , as prescribed by the Cahn-Hilliard equation, which describes the simplest form of phase separation for a conserved field [48]. The short-time dynamics can be further characterized by the cluster size histogram  $c_s(t) = n_s(t)/M$ , with  $n_s(t)$  the number of clusters of size  $s$ , displayed in Fig. 3(b). Assuming constant rate aggregation among clusters, one would show that, starting with an initial state only composed of individual particles,  $c_s(t) = \{[(t/t_2)^{p(s)}]/[(1 + t/t_2)^{q(s)}]\}$ , with  $p(s) = s - 1$  and  $q(s) = s + 1$  [49]. Here we find  $p(s) \simeq 0.6(s - 1)$  and  $q(s) \simeq s - 1$ . The observed differences, especially the fact that for  $t \gg 1$ ,  $c_s(t)$  decreases much slower than the prescribed  $1/t^2$ , indicate that the constant rate aggregation hypothesis does not hold:

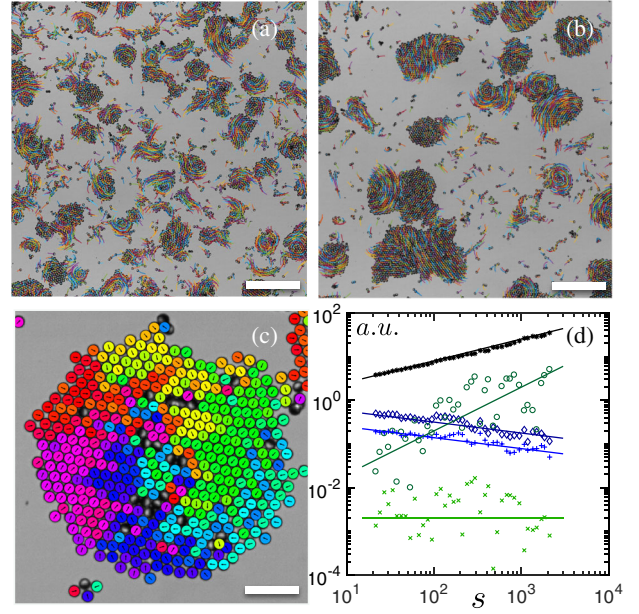


FIG. 4. Regime II, clusters dynamics: (a)–(b) Snapshots at times  $t = 8$  and  $t = 42$  s, with traces of the particles integrated over  $\Delta t = 0.4$  s. Scale bar is  $100 \mu\text{m}$ . (c) Enlargement on the colloid orientations inside one cluster. Scale bar is  $25 \mu\text{m}$ . (d) Cluster properties (in arbitrary units) as a function of cluster size  $s$ : (\*) radius of gyration  $R_G$ , (+) speed  $|\bar{v}|$ , ( $\diamond$ ) polarity  $|\bar{\Pi}|$ , ( $\times$ ) angular velocity  $\omega$ , and ( $\circ$ ) torque lever  $\tau/f_0$ . (see also the distributions in the Supplemental Material [45]).

aggregation process starts competing with evaporation and/or fragmentation events.

**Regime II: Aggregation-fragmentation.**—The onset of the second dynamical regime is initially marked by the slowing down of the aggregation process [Fig. 2(a)]. For  $t > 2$  s, most of the particles are already trapped within clusters. They form domains of locally aligned particles ( $\langle \pi \rangle$  is saturated). These domains point in random directions [Fig. 1(c)] and thereby prohibit large scale motion. Their size increases ( $\langle |\bar{\Pi}| \rangle$  slightly increases) until polar correlations reach the cluster size and, after another 2 s, new dynamics set in [Fig. 4(c)]: structural order develops, as indicated by the increase of both the hexagonal  $\langle \psi_{|6|} \rangle$  and hexatic  $\langle \psi_{|6|} \rangle$  order parameters, and the combination of local alignment and structural ordering leads to the emergence of rigid-body motion. The dynamics are heterogeneous—some clusters are static, other translate almost at the nominal speed of the individual colloids and others spin, like rigid bodies—and highly intermittent because collisions among the clusters redistribute the alignment of the colloids.

For a given cluster of size  $s$  at time  $t$ , we measure the velocity of each colloid  $\mathbf{v}_k = [\mathbf{r}_k(t + \Delta t) - \mathbf{r}_k(t)]/\Delta t$ , with  $\Delta t = 0.02$  s, and subsequently extract the position  $\bar{\mathbf{r}} = (1/s) \sum_{k=1}^s \mathbf{r}_k$ , velocity  $\bar{\mathbf{v}} = (1/s) \sum_{k=1}^s \mathbf{v}_k$  of the center of mass, the radius of gyration  $R_G = [(1/s) \sum_{k=1}^s |\mathbf{r}_k - \bar{\mathbf{r}}|^2]^{1/2}$  and the absolute angular rotation

$\omega = |(1/s) \sum_{k=1}^s \{[(\mathbf{r}_k - \bar{\mathbf{r}}) \times \mathbf{v}_k]/(|\mathbf{r}_k - \bar{\mathbf{r}}|^2)\}|$ . Here we assume each colloid exerts a force  $f_0 \mathbf{n}_k$  on the cluster it belongs to. Then the amplitude of the mean force exerted on a cluster of size  $s$  is simply  $f = f_0 |\mathbf{II}|$  and the amplitude of the mean torque is  $\tau = f_0 |(1/s) \sum_{k=1}^s (\mathbf{r}_k - \bar{\mathbf{r}}) \times \mathbf{n}_k|$ . Figure 4(d) shows how the radius of gyration, the translational and angular velocity, the mean force, and the mean torque scale with the cluster size:  $R_G \sim s^{0.5}$ ,  $v \sim s^{-0.25}$ ,  $\omega \sim s^{0.0}$ ,  $f \sim s^{-0.25}$ , and  $\tau \sim s^{1.0}$ . As a result, the translational drag coefficient  $\xi_t = (sf/v) \sim s^{1.0}$  while the rotational drag  $\xi_r = (s\tau/\omega) \sim s^{2.0}$ . Both scalings contrast with the Stokes prediction for a disk, ( $\xi_t \sim s^0 + \log$  corrections and  $\xi_r \sim s$ ), prohibiting the description of the cluster as a simple solid disk. The obtained scalings are, however, in agreement with the cumulative drag model proposed to describe active clusters [27]. These scaling laws are of crucial importance since they set the collision frequency amongst clusters, and thereby the temporal scaling of the coarsening dynamics. Within the limited range of dynamics we have access to, we propose the following bounds for the growth of the average cluster size:  $\langle s \rangle \sim t^{\gamma_2}$ , with  $\gamma_2 \in [2/3, 3/4]$  [see Fig. 2(a)]. On the theoretical side, there are very few cases where the master equation, governing the probability density of cluster sizes, can be solved exactly and one often restricts the description to the ‘‘monomer approximation’’ [27,50]. It is, however, clear that the present dynamics, which mainly involve cluster-cluster processes, would not be captured within such an approximation. Furthermore, the long timescale dynamics never take place, as we shall now see that the phase separation is anyway interrupted.

**Regime III : Interrupted phase separation.**—At long times, one would expect that most colloids aggregate into a few very large clusters ( $s \simeq 1000$ ), which eventually merge and form one dense droplet surrounded by a very dilute gas of individual colloids. Coarsening would then saturate because of the finite number  $M$  of colloids. The dynamics are actually far more complex, as evidenced by the large fluctuations observed in the temporal evolution of the mass-weighted average of the cluster size  $\langle m \rangle(t) = [(\sum_i s_i^2)/(\sum_i s_i)]$  [Fig. 5(a)]. Frequent very sharp breaking events take place, which, as we shall now argue, result from the imperfect aggregation of the clusters beyond a certain size.

Figure 5 displays the clusters colored with the three relevant local order parameters, namely, the hexagonal one [Fig. 5(b)], the hexatic one [Fig. 5(c)], and the polar one [Fig. 5(d)]. The clusters are typically hexagonally ordered (high local hexagonal order parameter) but do not form a unique crystalline domain, namely, a set of adjacent particles with the same value of the local hexatic order parameter. The interfaces separating the incoming clusters are thus populated with structural defects. The polar ordering is also not realized at the cluster scale and one clearly identifies separated sets of adjacent and aligned

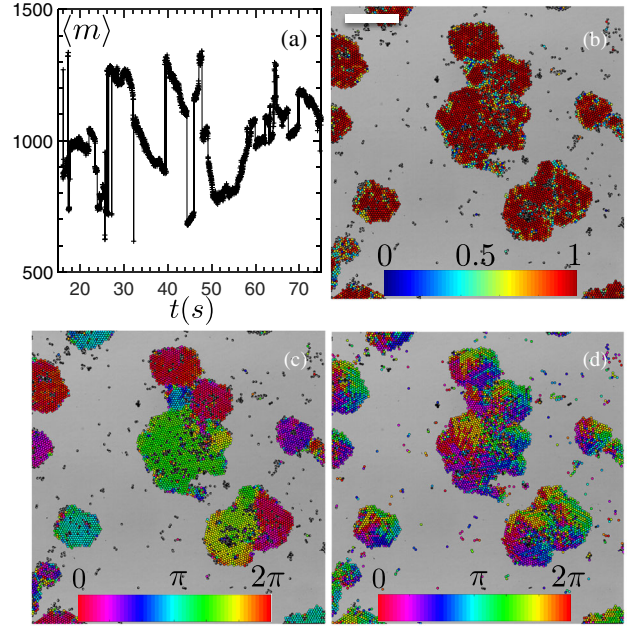


FIG. 5. Regime III, ordering within clusters: (a) Evolution of the mass-weighted average of the cluster size. Large clusters observed at time  $t = 20$  s with particles color coded by (b) the amplitude, (c) the argument of the local bond-orientational order parameter  $\psi_6$ , and (d) the orientation of their polar axis. Scale bar is  $100 \mu\text{m}$ . See also Movie-2,3,4 in the Supplemental Material [45].

particles. Not only the recently formed aggregate is not polar ordered, also the incoming clusters are not and present a few domains of aligned particles. The misalignment within the clusters is responsible for relative and disordered motion of the particles, leading to effective diffusion or superdiffusion, which in turn contributes to the healing of the interfaces populated with defects. This process is rather slow as evidenced by the slow growth of the hexatic order parameter  $\langle |\psi_6| \rangle$  [Fig. 2(c)]. It competes with the intense shear induced in the interfaces by the rotational and, to a lesser extent, translational motions of the incoming clusters. While the shear rate increases with the cluster size like  $R_G \omega$ , we expect the healing rate to decrease with the interface size, hence the cluster size. A critical size, above which coarsening is interrupted, is thus always reached, irrespective of the details of the healing mechanism. Altogether the advection induced coalescence is frustrated by the rotational induced shear. Additionally, we also observe spontaneous breakup of clusters. Both are promoted by the misbalanced of the aligned subdomains.

In summary, the coarsening dynamics result from the competition of three types of dynamics, that of motility induced phase separation, that of structural ordering, and that of polar alignment of the particles. The MIPS dynamics is initially the fastest one and rapidly leads to the formation of dense and compact clusters during the first regime. As long as the clusters are not too large, the structural ordering dynamics is fast enough compared to the aggregation rate

and the newly formed clusters rapidly become structurally homogeneous. Simultaneously, slower polar ordering develops spatial correlations at the cluster scale. These correlations are responsible for the presence of torques and forces, which in turn ensure the motility of the clusters and thereby set the aggregation rate during the second regime. In the last regime, the clusters have reached sizes such that the structural ordering now competes with the stresses inherited from the misalignment within the aggregating clusters. In this situation the long time state is very much reminiscent of the traffic jam and gliders reported in a simulations of active rods [5]. Depending on the relative growth rate of the three types of dynamics, one may expect different asymptotic states, leaving space for yet unexplored collective organizations. We therefore expect our work to motivate further numerical studies in the spirit of Ref. [30].

We thank Chantal Valeriani and Julien Tailleur for inspiring discussions and Jeroen Rijks for his contribution to the initial research. M.N. vdL. acknowledges support from the H2020 Marie Skłodowska-Curie Individual Fellowship “TOPACT.”

- 
- [1] F. Peruani, A. Deutsch, and M. Bär, *Phys. Rev. E* **74**, 030904(R) (2006).
- [2] F. Peruani, L. Schimansky-Geier, and M. Bär, *Eur. Phys. J. Spec. Top.* **191**, 173 (2010).
- [3] J. Deseigne, O. Dauchot, and H. Chaté, *Phys. Rev. Lett.* **105**, 098001 (2010).
- [4] M. E. Cates, D. Marenduzzo, I. Pagonabarraga, and J. Tailleur, *Proc. Natl. Acad. Sci. U.S.A.* **107**, 11715 (2010).
- [5] F. Peruani, T. Klaus, A. Deutsch, and A. Voss-Boehme, *Phys. Rev. Lett.* **106**, 128101 (2011).
- [6] F. Peruani, J. Starruß, V. Jakovljevic, L. Søgaard-Andersen, A. Deutsch, and M. Bär, *Phys. Rev. Lett.* **108**, 098102 (2012).
- [7] J. Schwarz-Linek, C. Valeriani, A. Cacciuto, M. E. Cates, D. Marenduzzo, A. N. Morozov, and W. C. K. Poon, *Proc. Natl. Acad. Sci. U.S.A.* **109**, 4052 (2012).
- [8] I. Theurkauff, C. Cottin-Bizonne, J. Palacci, C. Ybert, and L. Bocquet, *Phys. Rev. Lett.* **108**, 268303 (2012).
- [9] Y. Fily and M. C. Marchetti, *Phys. Rev. Lett.* **108**, 235702 (2012).
- [10] F. D. C. Farrell, M. C. Marchetti, D. Marenduzzo, and J. Tailleur, *Phys. Rev. Lett.* **108**, 248101 (2012).
- [11] R. Matas-Navarro, R. Golestanian, T. B. Liverpool, and S. M. Fielding, *Phys. Rev. E* **90**, 032304 (2014).
- [12] J. Palacci, S. Sacanna, A. P. Steinberg, D. J. Pine, and P. Chaikin, *Science* **339**, 936 (2013).
- [13] I. Buttinoni, J. Bialké, F. Kümmel, H. Löwen, C. Bechinger, and T. Speck, *Phys. Rev. Lett.* **110**, 238301 (2013).
- [14] M. E. Cates and J. Tailleur, *Europhys. Lett.* **101**, 20010 (2013).
- [15] G. S. Redner, M. F. Hagan, and A. Baskaran, *Phys. Rev. Lett.* **110**, 055701 (2013).
- [16] J. Stenhammar, A. Tiribocchi, R. J. Allen, D. Marenduzzo, and M. E. Cates, *Phys. Rev. Lett.* **111**, 145702 (2013).
- [17] B. M. Mognetti, A. Šarić, S. Angioletti-Uberti, A. Cacciuto, C. Valeriani, and D. Frenkel, *Phys. Rev. Lett.* **111**, 245702 (2013).
- [18] Y. Fily, S. Henkes, and M. C. Marchetti, *Soft Matter* **10**, 2132 (2014).
- [19] D. Levis and L. Berthier, *Phys. Rev. E* **89**, 062301 (2014).
- [20] J. Stenhammar, D. Marenduzzo, R. J. Allen, and M. E. Cates, *Soft Matter* **10**, 1489 (2014).
- [21] S. Weitz, A. Deutsch, and F. Peruani, *Phys. Rev. E* **92**, 012322 (2015).
- [22] E. Mani and H. Löwen, *Phys. Rev. E* **92**, 032301 (2015).
- [23] C. Tung, J. Harder, C. Valeriani, and A. Cacciuto, *Soft Matter* **12**, 555 (2016).
- [24] G. Liu, A. Patch, F. Bahar, D. Yllanes, R. D. Welch, M. C. Marchetti, S. Thutupalli, and J. W. Shaevitz, *Phys. Rev. Lett.* **122**, 248102 (2019).
- [25] A. Patch, D. Yllanes, and M. C. Marchetti, *Phys. Rev. E* **95**, 012601 (2017).
- [26] F. Alarcón, C. Valeriani, and I. Pagonabarraga, *Soft Matter* **13**, 814 (2017).
- [27] F. Ginot, I. Theurkauff, F. Detcheverry, C. Ybert, and C. Cottin-Bizonne, *Nat. Commun.* **9**, 696 (2018).
- [28] A. Martín-Gómez, D. Levis, A. Díaz-Guilera, and I. Pagonabarraga, *Soft Matter* **14**, 2610 (2018).
- [29] E. Sese-Sansa, I. Pagonabarraga, and D. Levis, *Europhys. Lett.* **124**, 30004 (2018).
- [30] X.-q. Shi and H. Chaté, [arXiv:1807.00294v2](https://arxiv.org/abs/1807.00294v2).
- [31] T. Vicsek, A. Czirók, E. Ben-Jacob, I. Cohen, and O. Shochet, *Phys. Rev. Lett.* **75**, 1226 (1995).
- [32] H. Chaté, F. Ginelli, and R. Montagne, *Phys. Rev. Lett.* **96**, 180602 (2006).
- [33] H. Chaté, F. Ginelli, G. Grégoire, and F. Raynaud, *Phys. Rev. E* **77**, 046113 (2008).
- [34] A. P. Solon, H. Chaté, and J. Tailleur, *Phys. Rev. Lett.* **114**, 068101 (2015).
- [35] J. Toner and Y. Tu, *Phys. Rev. E* **58**, 4828 (1998).
- [36] A. Peshkov, E. M. Bertin, F. Ginelli, and H. Chaté, *Eur. Phys. J. Spec. Top.* **223**, 1315 (2014).
- [37] M. E. Cates and J. Tailleur, *Annu. Rev. Condens. Matter Phys.* **6**, 219 (2015).
- [38] P. Ball, *Physics* **6**, 134 (2013).
- [39] E. Ben-Jacob, I. Cohen, and H. Levine, *Adv. Phys.* **49**, 395 (2000).
- [40] D. Kaiser, *Nat. Rev. Microbiol.* **1**, 45 (2003).
- [41] C. Dombrowski, L. Cisneros, S. Chatkaew, R. E. Goldstein, and J. O. Kessler, *Phys. Rev. Lett.* **93**, 098103 (2004).
- [42] Q.-X. Liu, A. Doelman, V. Rottschäfer, M. de Jager, P. M. J. Herman, M. Rietkerk, and J. van de Koppel, *Proc. Natl. Acad. Sci. U.S.A.* **110**, 11905 (2013).
- [43] D. Nishiguchi and M. Sano, *Phys. Rev. E* **92**, 052309 (2015).
- [44] J. Yan, M. Han, J. Zhang, C. Xu, E. Luijten, and S. Granick, *Nat. Mater.* **15**, 1095 (2016).
- [45] See Supplemental Material at <http://link.aps.org/supplemental/10.1103/PhysRevLett.123.098001> for reproducibility of the experiments.
- [46] S. Gangwal, O. J. Cayre, M. Z. Bazant, and O. D. Velev, *Phys. Rev. Lett.* **100**, 058302 (2008).

- [47] G. S. Redner, C. G. Wagner, A. Baskaran, and M. F. Hagan, *Phys. Rev. Lett.* **117**, 148002 (2016).
- [48] J. W. Cahn and J. E. Hilliard, *J. Chem. Phys.* **28**, 258 (1958).
- [49] P. L. Krapivsky, S. Redner, and E. Ben-Naim, *A Kinetic View of Statistical Physics* (Cambridge University Press, New York, 2010).
- [50] F. Peruani and M. Bär, *New J. Phys.* **15**, 065009 (2013).